Northumbria Research Link

Thin Film Flexible Acoustic Wave Devices with Off-axis Bending Characteristics for Multi-Sensing Applications

Zhangbin Ji[1], *Jian Zhou*[1,*], *Huamao Lin*[2], *Jianhui Wu*[1], *Dinghong Zhang*[1], *Sean Garner*[3], *Alex Gu*[2],*Shurong Dong*[4], *YongQing Fu*[5], *Huigao Duan*[1,*]

[1] College of Mechanical and Vehicle Engineering, Hunan University, Changsha 410082, China

[2] Shanghai Industrial μTechnology Research Institute (SITRI), 235 Chengbei Rd, Shanghai, 201800, China

[3]Corning Research & Development Corporation, One River Front Plaza, NY 14831, USA

[4]College of Information Science and Electronic Engineering, Zhejiang University, Hangzhou 310027, China

[5]Faculty of Engineering and Environment, Northumbria University, Newcastle upon Tyne, NE1 8ST, United Kingdom

*E-mail: jianzhou@hnu.edu.cn, duanhg@hnu.edu.cn

Abstract: Flexible surface acoustic wave (SAW) devices have recently attracted tremendous attention for their widespread applications in sensing and microfluidics. However, for these applications, the SAW devices often need to be bent into off-axis deformations between the acoustic-wave propagation direction and bending direction. Currently there are few studies on this topic, and the bending mechanisms under off-axis bending deformations have remained unexplored for multi-sensing applications. Herein, we fabricated aluminum nitride (AlN) flexible SAW devices by using high quality AlN films deposited on flexible glass substrates and systematically investigated their complex deformation behaviors. A theoretical model was firstly developed using coupling wave equations and boundary condition method to analyze the device's characteristics with bending and off-axis deformation under elastic strains. The relationships between frequency shifts of the SAW device with bending strain and off-axis angle were obtained which showed the identical results with those from the theoretical calculations. Finally, we performed proof-of-concept demonstrations of multi-sensing applications by monitoring human wrist movements at various off-axis angles and detecting

UV light intensities on a curved surface, thus paving the ways for versatile flexible electronics applications.

Keywords: flexible glass, SAW, frequency-strain, off-axis angle, sensors

1. Introduction

Acoustic wave devices (especially those based on surface acoustic wave, SAW) are attracting substantial interest as a sensing platform to detect physical, chemical and biological substances[1-3]. They offer merits such as high sensitivity, low detection limit (as the energy of the waves is mostly concentrated on the surface) and wireless-passive detection. They are also highly desirable for emerging technologies and integrated devices, including acoustofluidics[4,5], lab-on-chip[6], next-generation quantum communications [7], and integrated microwave-photonics signal processing[8]. Conventional SAW devices are fabricated on piezoelectric single crystal substrates, making them rigid and unsuitable for flexible electronics applications. This severely restricts their applications on a bent or curved surface of next-generation prosthetics, soft robotics, personalized healthcare systems and flexible printed circuits. This engineering challenge motivates the research on new materials, novel device architectures, and advanced manufacturing technologies.

Recently, to achieve mechanically robust, flexible and adaptive sensing microelectronics, flexible SAW devices with good flexibility and foldability are developed. In 2013, Jin et al fabricated flexible SAW sensing devices by depositing ZnO piezoelectric thin films on low-cost and commercially available polyimide (PI), demonstrating their excellent temperature sensing capability[9]. After that, various and flexible SAW applications including strain sensor[10,11], humidity sensor and respiration monitoring[12], UV sensor[13] and microfluidics[14] have been reported using polymer substrates, or metallic foil/sheet substrates. However, due to the significant dissipation of sound waves and energy, a low temperature tolerance and poor adhesion of thin films on the polymer substrates, it is a huge challenge to use these polymer-based thin film SAW devices for wide-range environment sensing (for example, high temperature environment), or high-performance microfluidics and lab-on-a-chip applications. On the other hand, metallic foils such as Al foils are easily plastically deformed without a good flexibility, as they are not easily recovered to their original states when they have been bent. In addition, both polymer and metallic foil based SAW devices have difficulties for wafer level

production, and they are incompatible with the IC process.

To address these limitations, Luo's group[15] and our group[16-17] reported flexible SAW device based on ZnO films on the flexible glass. Ultra-thin flexible glass is a suitable and inorganic substrate materials for flexible SAW devices as it has good bending-recoverable characteristics, low acoustic energy dissipation, excellent thermal and environmental stability, and capability of wafer-level production (up to 6-inch scale). However, the ZnO based SAW devices are not stable in acid and alkali extreme environment and high temperature environment[18], inhibiting their widespread applications. On the contrary, AlN film has a better mechanical and chemical stability and higher wave propagation velocity, and should be a suitable candidate for high performance sensors for applications in acid/alkali and high temperature environments[19]. However, AlN/ glass flexible based SAW devices have never been reported. In addition, there are few studies on the bending characteristics and mechanisms of the flexible SAW devices under different bending strains and off-axis deformations. There is also an urgent need to differentiate the effects of bending strain and off-axis angle of strain (along the acoustic-wave propagation direction and/or bending direction) on the device's sensing performance.

Herein, we fabricated AlN/glass flexible SAW devices by depositing high quality AlN films onto the flexible glass substrates as illustrated in Figure 1. A theoretical model was developed using coupling wave equation and boundary condition method to systematically analyze the bending and off-axis deformation characteristics of the flexible SAW devices under elastic strains (Figure 1(a)). Variations of frequency shifts were obtained with different bending strains, IDT periods and off-axis angles between the acoustic-wave propagation direction and bending direction. Results showed that the experimental results are identical to those from the theoretical calculations. To demonstrate the practical applications, the AlN/glass flexible SAW devices were applied to monitor the bending of human wrist. Furthermore, our flexible SAW sensors also demonstrate good capabilities for UV sensing on a curved substrate surface.

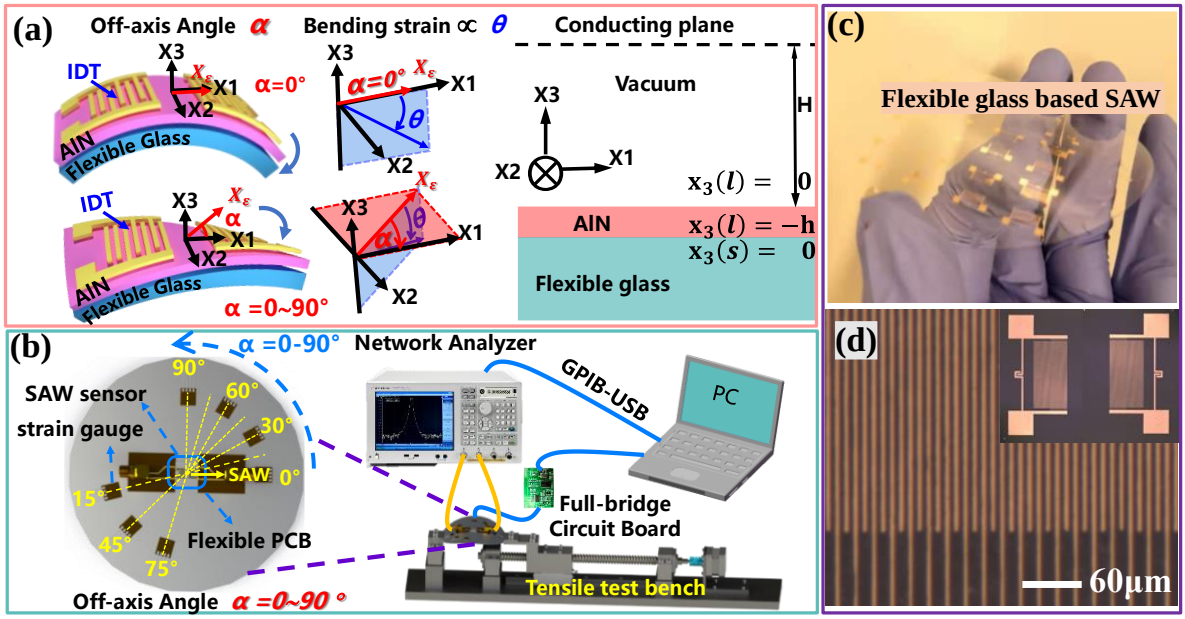

Figure 1. (a) Schematic diagrams of flexible and layered structure SAW devices at different off-axis angles α and bending strains (which is proportional to the bending angle θ); (b) An schematic view of the strain testing system used for flexible SAWs at various off-axis angles α; (c) The fabricated flexible SAW device on an ultrathin flexible glass substrate, showing good flexibility and wafer-scale level; (d) Microscopic images of fabricated flexible SAW devices, showing the whole device and well-defined IDTs with a periodicity of 20 μm.

2. Bending Modeling and Off-axis Deformation of Flexible SAW devices

We firstly used coupling wave equations and boundary condition methods to systematically analyze the bending and off-axis deformation characteristics under elastic strains for flexible glass based SAW devices.

Frequency of the flexible SAW device changes with its bending and off-axis deformation due to the strain-induced changes in both SAW velocity and wavelength (due to IDT deformation in the direction of SAW propagation). To investigate these in details, the above two components are considered independently. The velocity changes under the applied stress can be calculated by a modified form of equations of motion which considers the perturbation of applied strains [20]. When an AlN/flexible glass layered device is under a bending strain, the coupling wave equations are[21]

$$\sigma_{jk}\frac{\partial^2 u_i}{\partial x_j \partial x_k} - \rho\frac{\partial^2 u_i}{\partial t^2} + C_{ijkl}\frac{\partial^2 u_k}{\partial x_l \partial x_j} + e_{jkl}\frac{\partial^2 \phi}{\partial x_k \partial x_j} = 0 \quad (1)$$

$$e_{jkl}\frac{\partial^2 u_k}{\partial x_l \partial x_j} - \varepsilon_{jk}\frac{\partial^2 \phi}{\partial x_k \partial x_j} = 0 \quad (2)$$

where i, j, k, l = 1, 2, 3, the Einstein summation convention is indicated by repeated indices;

σ_{jk} is the initial stress; u the mechanical displacement; ρ the density; φ the electrical potential; C_{ijkl}, e_{jkl}, ε_{jk} are elastic stiffness constants, piezoelectric constants and dielectric constants, respectively.

A solution for the displacement vector of AlN/glass flexible SAW device is a linear combination of fundamental solutions in a form of[20]

$$u_k = e^{j\omega t}\beta_k exp\left[-j\frac{w}{v}(x_1 + \gamma x_3)\right] \quad (k = 1,2,3,4) \tag{3}$$

where γ is a complex normalized transverse wave number, v is the acoustic wave velocity. Here, u_4 represents electrical potential φ.

By substituting Eq. (3) into Eq. (1) and (2), and ignoring the effects of horizontal shear waves due to the type of crystal structure of AlN (with its dominant (0002) orientation) and flexible glass, we then obtain the simplified Christoffel equations for AlN piezoelectric layer and flexible glass substrate, as shown in Eq.(4) and Eq.(5), respectively.

$$\begin{bmatrix} \Gamma_{11} - \rho v^2 & \Gamma_{13} & \Gamma_{14} \\ \Gamma_{13} & \Gamma_{33} - \rho v^2 & \Gamma_{34} \\ \Gamma_{14} & \Gamma_{34} & \Gamma_{44} \end{bmatrix} \begin{bmatrix} \beta_{1(L)} \\ \beta_{3(L)} \\ \beta_{4(L)} \end{bmatrix} = 0 \tag{4}$$

$$\begin{bmatrix} \Gamma_{11} - \rho v^2 & \Gamma_{13} \\ \Gamma_{13} & \Gamma_{33} - \rho v^2 \end{bmatrix} \begin{bmatrix} \beta_{1(s)} \\ \beta_{3(s)} \end{bmatrix} = 0 \tag{5}$$

The determinants of these five equations with three variables $\beta_{1(L)}, \beta_{3(L)}, \beta_{4(L)}$ and another two variables $\beta_{1(S)}, \beta_{3(S)}$ must be zero for nontrivial solutions. We can then obtain a six-order polynomial equation and a four-order polynomial equation in γ. In the piezoelectric material layer, there are six different roots of ${\gamma_L}^{(q)}$, q= 1 to 6, and all these six ${\gamma_L}^{(q)}$ are useful. In the substrate layer, there are four different roots of ${\gamma_L}^{(q)}$, q= 1 to 4, and two values of ${\gamma_s}^{(q)}$, for which $Im{\gamma_s}^{(q)}>0$ are allowed because of the attenuation of the acoustic wave in the substrate. For each ${\gamma_L}^{(q)}$, the relevant $\beta_{(L)k}$ can be obtained.

Based on these, the complete solutions for both the piezoelectric layer and substrate can be given by,

$$u_k(L) = \sum_{q=1}^{Q(L)} e^{j\omega t} B_{(L)}^{(q)} \beta_{k(L)}^{(q)} exp\left[-j\frac{w}{v}\left(x_1 + \gamma^{(q)} x_3\right)\right], \quad Q(L) = 6 \tag{6}$$

$$u_k(S) = \sum_{q=1}^{Q(S)} e^{j\omega t} B_{(S)}^{(q)} \beta_{k(S)}^{(q)} exp\left[-j\frac{w}{v}\left(x_1 + \gamma^{(q)} x_3\right)\right], \quad Q(S) = 2 \tag{7}$$

To obtain the acoustic wave velocity, four boundary conditions are given [20] and shown in the SI materials. The four boundary conditions can form a set of 8 homogeneous equations (SI materials) for two variables $B_{(S)}^{(q)}$ and six variables $B_{(L)}^{(q)}$. The determinants of these equation sets should be zero for nontrival solutions. Then a transcendental equation for the determination of *v* is obtained. An iterative process was further used in the computation to find the value of v.

When the applied strain is a perturbation to the propagating SAW, the applied strain not only modifies the equation of motion, but also changes the material constants. There are three independent perturbed material constants influencing the acoustic velocity under stress [21], which are the initial stress (σ_{ij}), material elastic constants (C_{ijkl}), and material density (ρ). The original parameters were substituted with these changed ones to calculate the velocity changes under different strains and applied off-axis angles.

A MATLAB program was developed to conduct the iteration calculation of SAW velocities as a function of applied strain. The strain sensitivity (S) is defined as

$$S = \frac{\Delta f}{\Delta \varepsilon} = \frac{(\Delta v/v - \Delta\lambda/\lambda).f_0}{\Delta \varepsilon} \tag{8}$$

where f_0 is the resonant frequency under zero strain. All the results of the detailed theoretical calculation are provided in the SI materials.

3. Experimental Section

The flexible SAW devices were fabricated on flexible Corning® Willow® Glass substrates (100 μm in thickness and 75 mm in diameter) as illustrated in Figure 1(b). Piezoelectric AlN films were deposited onto the flexible glass substrates using a reactive magnetron sputtering system with a pure Al target and a gas mixture of N_2/Ar. The optimal deposition conditions were: a substrate temperature of 200 °C, a deposition pressure of 0.43 Pa, and a N_2/Ar gas ratio of 1:5. The target pulsed DC power was 10 kW and the RF bias power was 160 W. Crystal orientation of the AlN film was characterized using X-ray diffraction (XRD-6000) with a Cu-*Kα* radiation source and a scanned angle of 2*θ* =20°~70°. Crystallite sizes were calculated using the Debye–Scherrer formula based on the full width at half maximum (FWHM) of the AlN diffraction peak (*β* in radians): $D=K\lambda/(\beta cos\theta)$[16], where *K* is

the shape factor of the average crystallite with a value of 0.94, λ the X-ray wavelength (1.5405 Å for Cu target), θ the Bragg angle, and D the mean crystallite gain size normal to diffracting planes. Residual strain of the film was calculated from $\varepsilon_z = (c-c_0)/c_0$[16], where c_0 is the strain-free lattice constant and c the lattice constant which is equal to twice of the inter-planar spacing d, measured from the position of the (0002) peak using the Bragg equation. Scanning electron microscope (SEM, Sigma-300, ZEISS, Germany), atomic force microscope (AFM, Dimension Icon, Bruker) and transmission electron microscope (TEM, JEM-2100Plus, JEOL, Japan) were applied to characterize cross-section morphologies, surface topography and lattice structure of the AlN films.

Conventional photolithography and lift-off processes were used to fabricate AlN/glass based flexible SAW devices with different wavelengths (λ) of 12, 16, 20 and 24 μm. The flexible SAW device has 50 pairs of IDTs with a metallization ratio of 0.5, reflectors of 100 pairs, an aperture length of 200 λ, and the center distance between the two ports of 150 λ. Figure 1b shows an optical image of the fabricated AlN/glass based flexible SAW device, demonstrating its good flexibility and uniform interdigitated structure.

For bending tests, the fabricated SAW devices were diced into small devices (1.5×1.5 cm) from the glass wafer, as shown in Figure 1(b), and then bonded onto a 1 mm thick stainless steel plate using ethyl α-cyanoacrylate adhesive (No.502 glue). They were then electrically connected to the flexible printed circuit board (PCB, which was mounted onto steel plate) using the conductive silver paste. A tensile tester was used to bend the steel plate and apply the bending strain to the flexible SAW device. To investigate the effect of off-axis angle (e.g., the angle between the acoustic-wave propagation direction and the bending direction) on the frequency responses of flexible SAW devices, we set the off-axis angles at 0°, 15°, 30°, 45°, 60°, 75°and 90°, respectively, by rotating the stainless steel plate. Therefore, the strain was applied to the surface acoustic wave device in different off-axis directions. Seven standard strain gauges were glued near to the SAW sensor, which provided the strain readings and calibrated the dynamic strains. The transmission spectra of the flexible SAW devices were obtained using a vector network analyzer (3656D, Ceyear, China), and a LabVIEW program was developed to automatically record the frequency changes as a function of time at different bending strains and off-axis angles.

4. Results and Discussion

Figure 2(a) is the XRD pattern of the AlN film, which shows a single peak at the angle of ~36°, corresponding to the AlN (0002) crystal orientation. The full width at half maximum (FWHM) is 0.281°, corresponding to the calculated mean grain size of about 29.7 nm. The axial stress of the film was estimated to be 42.25 MPa based on the lattice constant obtained through XRD patterns, exhibiting that the deposited film has a low tensile residual stress on the flexible glass substrate. Fig. 2(b) is a cross-section SEM picture of AlN film on flexible glass, which shows a vertically columnar structure. Figure 2(c) is a high resolution TEM (HRTEM) image and its corresponding fast Fourier transformation (FFT) image (inset) of the AlN film on the flexible glass, revealing that the AlN grains are well textured along the (0002) orientation Figure 2(d) shows the surface morphology and roughness of the film obtained using the AFM. The root mean square (RMS) roughness was measured to be 7.64 nm over an area of 4×4 μm^2. The preferred c-axis orientation, low residual stress and small value of roughness of the AlN films are critical for high-performance flexible SAW devices.

Figure 2(e) shows a survey spectrum of the AlN films obtained using an X-ray photoelectron microscopy (XPS), in which the photoelectron peaks of Al, N, C and O elements can be detected. The N 1s and Al 2p peaks in the XPS spectra confirm the formation of Al-N structures[22,23]. The binding states of these elements were further investigated using the XPS, and the results are shown in Fig. 2(f). Two binding energy components of N1s were obtained after the peak deconvolution using a curve-fitting program. The peak at a binding energy of 397.09 eV corresponds to the aluminum–nitrogen (Al-N) bonds. This energy agrees well with the previously published values for the AlN films[22]. For the binding-energy spectrum of Al 2p, two peaks at binding energies of 74.4 and 73.8 eV were deconvoluted for the best fitting of the spectrum. The lower binding energy (73.8 eV) component can be attributed to aluminum in AlN[23]. The Al 2p peak which appears at 74.4 eV corresponds to aluminum in its oxide states[24]. The formation of a protective layer of aluminum oxides on the surface of AlN when exposed to the atmosphere has been well documented[25].

Transmission (S_{21}) spectra of the flexible SAW devices with different wavelengths are

shown in **Figure S1.** All these flexible SAW devices show well-defined Rayleigh resonant peaks. The resonant frequencies are 290.1MHz, 211.8 MHz, 166.9 MHz, and 139 MHz for the SAW devices with wavelengths of 12, 16, 20 and 24 μm, respectively. The phase velocities (v_p) of these SAW devices, $V_p = \lambda f$, were calculated to be 3481.50, 3388.32, 3340.40 and 3336.24 $m \cdot s^{-1}$, respectively, decreasing gradually with an increase in wavelength from 12 to 24 μm. When the wavelength is increased, more energy is dispersed into the flexible glass (3200 $m.s^{-1}$), which has a lower velocity of wave propagation than that of AlN film (~5600 $m.s^{-1}$), thus

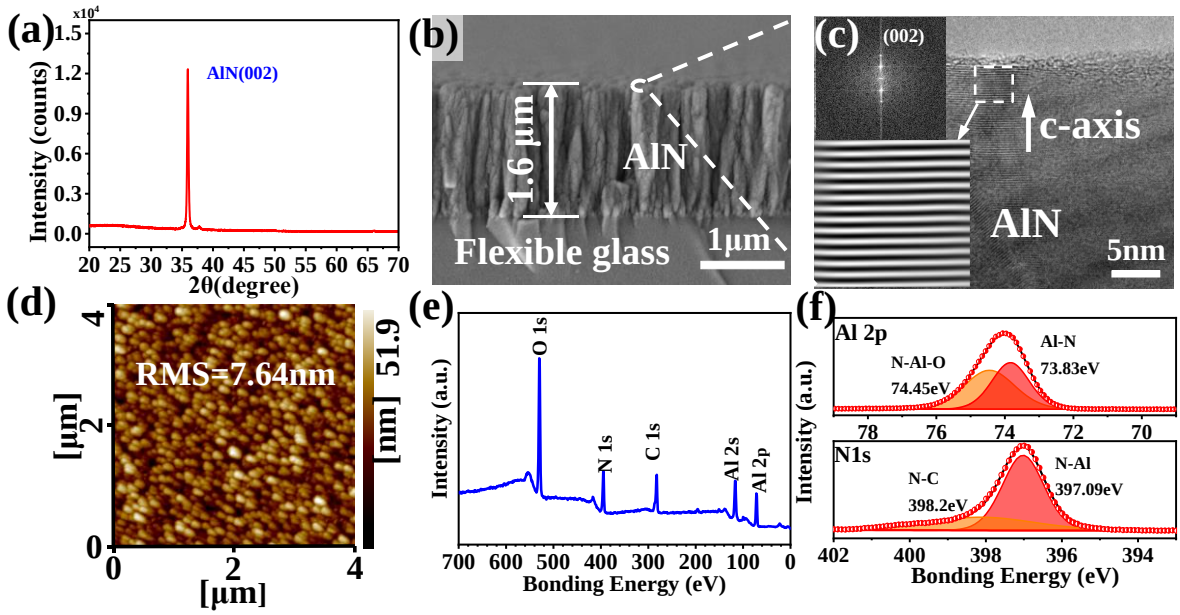

leading to a lower velocity of waves in the layered structure. Discussions of device performance between our flexible AlN/glass SAW devices with the previous flexible SAW devices are shown in the SI materials.

Figure 2. Characterization of AlN thin film deposited on the flexible glass substrate: (a) XRD pattern of the AlN film on flexible glass, showing strong (0002) orientation; (b) SEM image of the cross-section of the AlN film on flexible glass; (c) HRTEM image of AlN film, and the inset figure is FFT image; (d) AFM image of the AlN film on flexible glass, showing the smooth surface; (e) XPS survey spectrum of the AlN films on flexible glass; (f) XPS high-resolution spectra of Al 2p and N 1s of the AIN films.

Bending and off-axis deformation characteristics of flexible SAW device. The electromechanical responses of the flexible SAW device (with a wavelength of 20 μm) as a function of applied strain from zero to 1332 με and then to its full recovery state is shown in Fig. 3(a). Results show that the frequency change of flexible SAW device is linearly correlated with the applied strain. The calculated linear regression coefficient is ~0.99967, showing an excellent linearity, based on which the strain-sensitivity was calculated to be 99.5 Hz/με. For

frequency-strain recovery in one cycle, its maximum hysteresis of the flexible SAW device is less than 0.24 %, which is much better than the reported value for the flexible SAW devices [11].

To investigate the effects of the wavelength on the frequency-strain responses, the flexible SAW devices with different wavelengths have been applied with different bending strains, and the obtained frequency results are shown in Figure 3(b). The corresponding strain-sensitivity data were calculated to be 180.08, 130.29, 99.50 and 64.38 Hz/με, for the devices with the wavelengths of 12, 16, 20 and 24 μm, respectively. This indicates that the strain-sensitivity of AlN/glass based flexible SAW devices decreases significantly with the increase in wavelength, mainly due to the decreased resonant frequency. We have also theoretically analyzed the effects of SAW wavelength on the strain-frequency responses, and the results are shown in Figure S3(a). The calculated strain-sensitivities are in good agreements with the experimental results, as illustrated in Figure 3(c).

Figure 3(d) shows frequency shifts of the flexible AlN SAW devices as the functions of bending strain, with different off-axis angles of 0, 15°, 30°, 45°, 60°, 75° and 90°, respectively. It is obvious that the frequency-strain responses of flexible SAW devices still exhibit a good linearity at different off-axis angles and the obtained frequency-strain sensitivity decreases with the increase of the off-axis angle α. The theoretical results of frequency shifts as functions of bending strain and off-axis angle α are shown in Figure S3(b), which are well consistent with the experimental data, as illustrated in Fig. 3(e). An interesting phenomenon is that when the off-axis angle α is 90°, the frequency variation is different with those with the other off-axis angles. Previously a study on ZnO/glass SAW device also reported this phenomenon, which was attributed to the experimental error[26]. However, our flexible SAW devices with different wavelengths present the same trend, indicating that it should be a real phenomenon.

To understand the mechanisms behind this phenomenon, we have theoretically calculated the frequency-strain responses of AlN/glass flexible device (λ=20 μm), by considering the initial stress, elastic constant and density, which are three key factors leading to apparent changes of SAW velocity. We then calculated the frequency-strain responses due to the IDT deformation (e.g, changes of IDT dimensions) in the direction of SAW propagation, and also the combined effects due to all the above factors. The results are shown in Figures 3(f) and 3(g). When the off-axis angle α is 0°, the IDT deformation causes a negative frequency shift,

but the combined effect of IDT deformation and change of SAW velocity leads to a positive frequency shift. When the off-axis angle α is 90°, even though the IDT deformation causes a positive frequency shift, but the combined effect leads to a negative frequency shift. These results clearly demonstrate that the frequency shift is mainly due to the changes of SAW velocity but not IDT deformation. In addition, both the initial stress and change of density will lead to a positive frequency shift, while the changes of elastic constants cause a negative frequency shift for the off-axis angle α between 0 and 90°.

Clearly the changes in acoustic velocity depend on the combined effect of all these three factors (e.g., initial stress, density and the elastic constants), and could be positive or negative. When the off-axis angle α is 0°, the main contribution factor on the frequency-strain shift is the initial stress (Figure 3(f)). However, when the off-axis angle α is increased from 0° to 90°, the contribution of initial stress on the positive frequency-strain shift is decreased remarkably, while the effects of elastic constants and density on the frequency-strain shifts are only changed slightly. Therefore, the combined effect will lead to frequency changed from a positive value to a negative one when the off-axis angle α is increased from 0° to 90°.

Figures S4(a) & S4(b) show the variations of insertion losses of the flexible SAW device as functions of bending strain and off-axis angle α at different wavelengths. The insertion loss of flexible SAW devices has not shown obvious changes during the bending process, showing the good stability of AlN/flexible glass based SAW devices under the bending and off-axis deformation.

To investigate the long-term stability and fatigue failure of the flexible SAW devices in real-life applications, they were repeatedly bent/released for more than 1300 cycles with a maximum applied strain of 1000 με. Figure 3 (h) shows the obtained frequency shifts at three stages: e.g., beginning stage (0–1000s), after 9 hours (36400s-37400s), and near to the end (64800s-65800s) under the cyclic bending test. The SAW device's performance (e.g., frequency shifts) has not shown apparent changes. These results verify that the fabricated flexible SAW device has good mechanical durability and stability, demonstrating its great potential for flexible electronics applications.

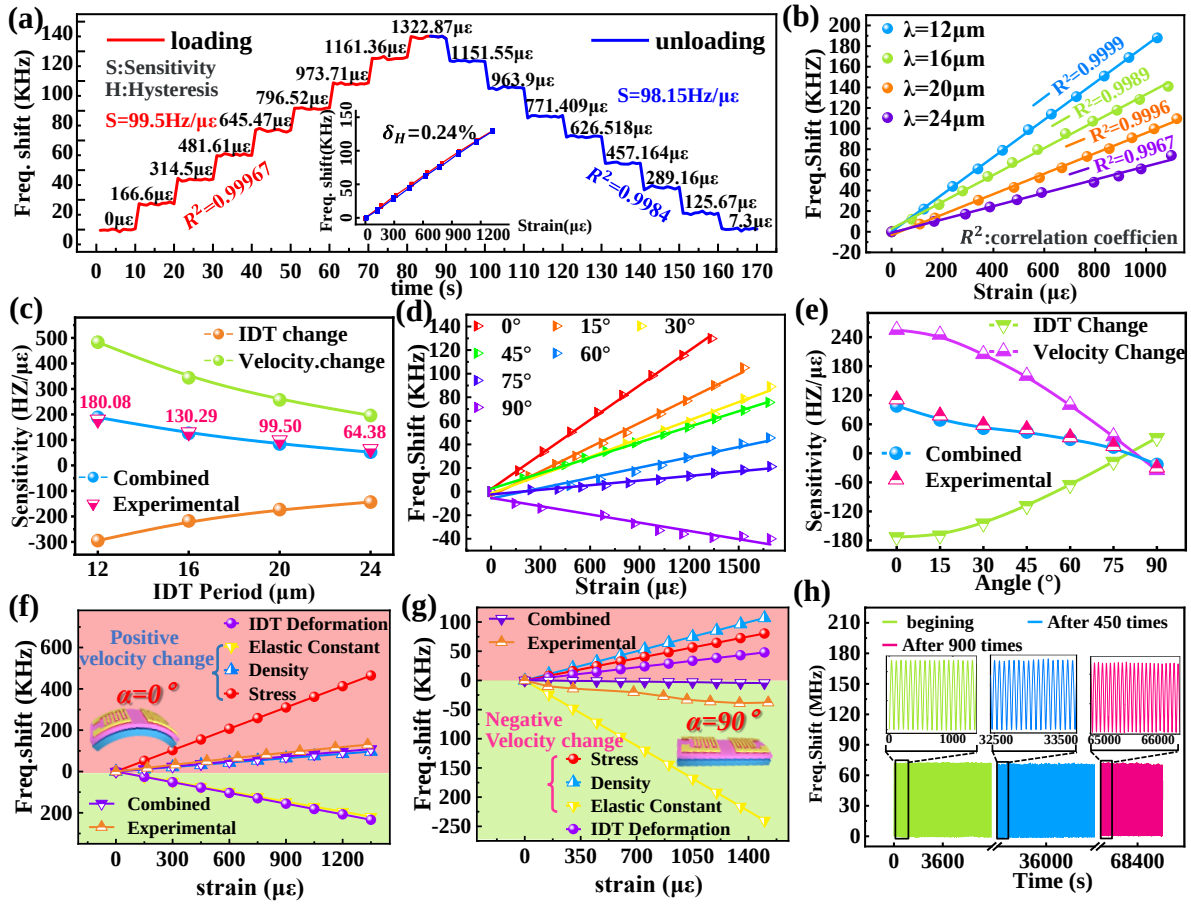

Figure 3. (a) Resonant frequency responses of the flexible SAW device to the applied strains from 0 to 1322 με in both loading and unloading conditions, and the inset shows an excellent linearity and small hysteresis of the frequency responses; (b) Resonant frequency shifts as a function of strain for flexible SAWs at different IDT wavelengths; (c) Comparisons between experimental strain sensitivities and theoretically calculated strain sensitivities (induced by velocity change, IDT deformation and their combined effect) at different IDT periods; (d) Resonant frequency shifts as a function of strain for flexible SAW at different off-axis angles α; (e) The comparison between experimental strain sensitivities and theoretical calculated strain sensitivities as a function of off-axis angle α; (f) and (g) The comparisons between experimental frequency shifts and theoretical calculated frequency-strain responses (induced by the initial stress, elastic constants, density and IDT deformation), at the off-axis angles of α=0° and α=90°, respectively, for the AlN/flexible glass SAW device with λ=20 μm; (h) Frequency responses of the fabricated flexible SAW devices under cyclic bending test.

Human motion detection and UV sensing on the curved surface. To verify the proposed model for the flexible SAW device under bending and off-axis deformation, and demonstrate the practical applications of our flexible SAW sensors, an AlN/glass flexible sensor was attached onto the wrist of a volunteer (with the off-axis of 0°, 30°, 60 °) to detect bending of the wrist. The obtained results are shown in Figure 4a. Results show that the frequency shifts of the flexible SAW device increase with the increase of bending angle of wrist,

mainly due to increases of the strains. Furthermore, with the off-axis angle (α) increased from 0°, 30°, to 60°, the frequency shifts are reduced at the given bending strain. This is mainly due to the lower frequency-strain sensitivity at a higher off-axis angle, which is well agreeable with the strain analysis results shown above.

To demonstrate the sensing performance of flexible SAW devices which are applied onto the curved and complex surfaces, the AlN/glass device, which was pre-coated with ZnO nanowires (purchased from XFNANO, Nanjing, China) onto the AlN film surface in order to enhance the absorption of UV lights, was bonded onto a flat steel plate. The steel plate was under a flat state or was bent with a strain of 1000 με with the off-axis angles of 0, 30, and 60°. Detection of the UV source (with a wavelength of 365 nm and intensity of 35 mw/cm^2) was performed using the above device at different bending conditions and the obtained results are shown in Figure 4(c). Results show that the off-axis angle α and bending strain will affect the starting/resonant frequency of the flexible SAW device, but the UV performance is almost the same and does not have obvious differences for all the cycling tests. Our results demonstrated that the fabricated SAW device can work well at different off-axis angles α and bending strains, and has shown a comparable UV sensing performance compared with those on the flat plate surface.

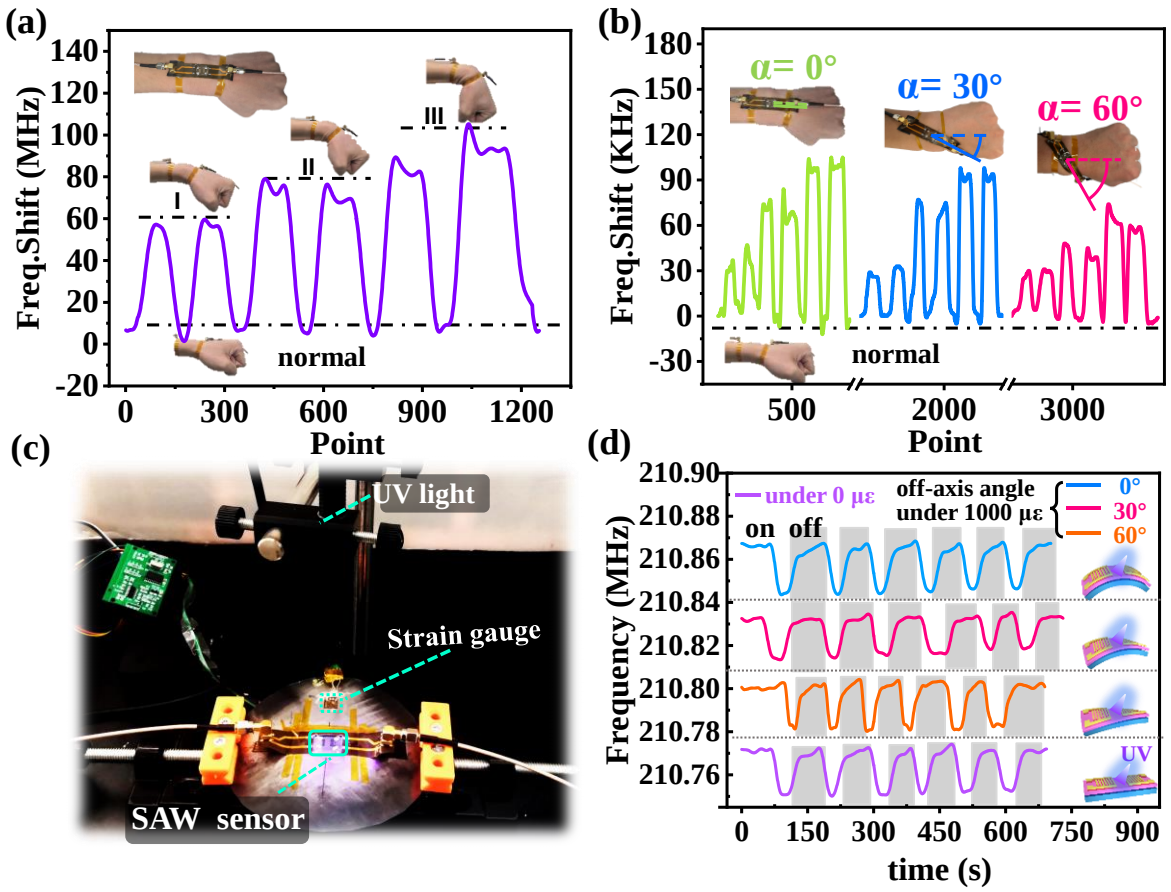

Figure 4 (a) Frequency shifts of the flexible SAW devices under different wrist bending states; (b) Frequency shifts of the flexible SAW devices under three wrist bending states at the off-axis angles α of 0, 30, and 60°; (c) Illustration of the experimental setup for ultraviolet detection on a curved surface using the flexible SAW sensor; (d) Frequency responses of our flexible SAW device to UV light (UV wavelength of 365 nm and intensity of 35mw/cm²), under the strains of 0 με and1000 με, with the off-axis angles α of 0, 30, and 60°.

It is worthwhile to note that the frequency shifts are related to both the bending strain and off-axis angle. To distinguish the individual effect of these two parameters on the frequency responses, we can use a pair of identical SAW devices, which are orthogonally positioned onto the sensing area. After applying a bending strain and an off-axis deformation to the area, these two orthogonal SAW devices will produce different frequency shift results. We can solve/decouple from the individual frequency shifts of these two orthogonal SAW devices, and identify the effects of bending strain and off-axis deformation.

Conclusion

In this work, we developed AlN/ glass flexible SAW devices by using high quality AlN films on the flexible glass substrates. A theoretical model was firstly developed using coupling

wave equation and boundary condition method to systematically analyze the bending and off-axis deformation characteristics of the flexible SAW devices under an elastic strain. The functions of frequency shifts on different bending strains and off-axis angles were obtained, and the results are in good agreements with those from the theoretical calculation. We performed proof of concept demonstrations by detecting human wrist bending at various off-axis angles and sensing UV light changes on the curved surface, and proved the device's great potentials for versatile and flexible electronics applications.

ASSOCIATED CONTENT

Supporting Information

AUTHOR INFORMATION

Corresponding Author

Jian Zhou − College of Mechanical and Vehicle Engineering, Hunan University, Changsha 410082, China; Email: jianzhou@hnu.edu.cn

Huigao Duan − College of Mechanical and Vehicle Engineering, Hunan University, Changsha 410082, China; Email: duanhg@hnu.edu.cn

Author Contributions

The manuscript was written through contributions of all authors. All authors have given approval to the final version of the manuscript.

Notes

The authors declare no competing financial interest.

Ethics Approval was granted by Ethics Committee of College of Biomedical Engineering and Instrument Science from Zhejiang University, Reference Number 7, with a valid period of 2 years.

ACKNOWLEDGMENTS

This work was supported by the General Program of National Natural Science Foundation of China (NSFC No.52075162), Innovation Leading Program of New and High-tech Industry of Hunan Province (2020GK2015), the Natural Science Foundation of Changsha (kq2007026), the Key Research Project of Guangdong Province (2020B0101040002), the Engineering Physics and Science Research Council of UK (EPSRC EP/P018998/1) and International Exchange Grant (IEC/NSFC/201078) through Royal Society and the NSFC. We also thank the Shaomin Zhang from Zhejiang University for the IRB approval.

REFERENCES

1 Zheng, J. P. et al. 30 GHz surface acoustic wave transducers with extremely high mass sensitivity. *Appl. Phys. Lett.* **116**, 123502 (2020)

2 Chen, Z. et al. Ultrahigh-frequency surface acoustic wave sensors with giant mass-loading effects on electrodes. *ACS Sens.* **5**, 1657-1664 (2020)

3 Lamanna, L. et al. Conformable surface acoustic wave biosensor for E-coli fabricated on PEN plastic film. *Biosens. Bioelectron*. **163**, 112164 (2020)

4 Gu, Y. et al. Acoustofluidic centrifuge for nanoparticle enrichment and separation. *Sci. Adv*. **7**, eabc0467 (2021)

5 Chen, C. Y. et al. Acoustofluidic rotational tweezing enables high-speed contactless morphological phenotyping of zebrafish larvae. *Nat. Commun.* **12**, 1118 (2021)

6 Fu, Y. Q. et al. Engineering inclined orientations of piezoelectric films for integrated acoustofluidics and lab-on-a-chip operated in liquid environments. *Lab Chip* **21**, 254-271 (2021)

7 Satzinger, K. J. et al. Quantum control of surface acoustic-wave phonons. *Nature* **563**, 661-665 (2018)

8 Munk, D. et al. Surface acoustic wave photonic devices in silicon on insulator. *Nat. Commun.* **10**, 4214 (2019)

9 Jin, H. et al. Flexible surface acoustic wave resonators built on disposable plastic film for electronics and lab-on-a-chip applications. *Sci. Rep.* **3**, 2140 (2013,)

10 Li, Q. et al. Highly Sensitive Surface Acoustic Wave Flexible Strain Sensor. *IEEE Electron Device Lett.* **40**, 961-964 (2019)

11 Xu, H. et al. Flexible surface acoustic wave strain sensor based on single crystalline LiNbO3 thin film. *Appl. Phys. Lett.* **112**, 093502 (2018)

12 Wang, C. et al. Programmable and scalable transfer printing with high reliability and efficiency for flexible inorganic electronics. *Sci. Adv*. **6**, eabb2393 (2020)

13 He, X. L. et al. High performance dual-wave mode flexible surface acoustic wave resonators for UV light sensing. *J. Micromech. Microeng.* **24**, 055014 (2014,)

14 Tao, R. et al. Hierarchical Nanotexturing Enables Acoustofluidics on Slippery yet Sticky, Flexible Surfaces. *Nano Lett.* **20**, 3263-3270 (2020,)

15 Chen, J. K. et al. Bendable transparent ZnO thin film surface acoustic wave strain sensors on ultra-thin flexible glass substrates. *J. Mater. Chem. C* **2**, 9109-9114 (2014)

16 Yin, C.S. et al., Enhancing the sensitivity of flexible acoustic wave ultraviolet photodetector with graphene-quantum-dots decorated ZnO nanowires. *Sens. Actuators, A.* **321**, 112590 (2021).

17 Wu, J. H. et al. Ultrathin Glass-Based Flexible, Transparent, and Ultrasensitive Surface Acoustic Wave Humidity Sensor with ZnO Nanowires and Graphene Quantum Dots. *ACS Appl. Mater. Interfaces* **12**, 39817-39825 (2020)

18 Xiong, S. et al. Stability studies of ZnO and AlN thin film acoustic wave devices in acid and alkali harsh environments. *RSC Adv.* **10**,19178-19184 (2020)

19 Lin, C. M. et al. Thermally compensated aluminum nitride Lamb wave resonators for high temperature applications. *Appl. Phys. Lett.* **97**, 3 (2010,)

20 Nalamwar, A. l. et al. Effects of Applied Strain in ZnO Thin-Film. *IEEE Trans. Sonics Ultrason* **23**, 144-147 (1976)

21 Nalamwar, A. L. et al. Surface acoustic waves in strained media. *J. Appl. Phys.* **47**, 43-48 (1976).

22 Wang, P. W. et al. Aluminum nitride and alumina composite film fabricated by DC plasma processes. *Thin Solid Films* **295**,142-146 (1997)

23 Martin, P. et al. Optical properties and stress of ion-assisted aluminum nitride thin films. *Appl. Opt.* **31**, 6734-40.(1992)

24 Strite; S. et al. GaN, AlN, and InN: *J. Vac. Sci. Technol. B* **10**, 1237 (1992)

25 Dimitrova, V. I. et al. Study of reactive DC magnetron sputtering deposition of AlN thin films. *Vacuum* **49**, 193-197 (1998)

26 Chen, J. et al., Development of flexible ZnO thin film surface acoustic wave strain sensors on ultrathin glass substrates. *J. Micromech. Microeng.* **25**, 115005 (2015)